Pergamon

Geochimica et Cosmochimica Acta, Vol. 68, No. 10, pp. 2207–2221, 2004

0016-7037/04 $30.00 + .00

doi:10.1016/j.gca.2003.12.010

Experimental determination of synthetic $NdPO_4$ monazite end-member solubility in water from 21°C to 300°C: Implications for rare earth element mobility in crustal fluids

Franck Poitrasson,* Eric Oelkers, Jacques Schott, and Jean-Marc Montel

Laboratoire d'étude des Mécanismes de Transfert en Géologie, CNRS, 14, Avenue Edouard Belin, 31400 Toulouse, France

(*Received August* 20, 2003; *accepted in revised form December* 4, 2003)

Abstract—The solubility of synthetic $NdPO_4$ monazite end-member has been determined experimentally from 21 to 300°C in aqueous solutions at pH = 2, and at 21°C and pH = 2 for $GdPO_4$. Measurements were performed in batch reactors, with regular solution sampling for pH measurement, rare earths and phosphorous analysis by inductively coupled plasma mass spectrometry (ICP-MS) coupled with a desolvation system. Scanning electron microscopy (SEM) and X-ray photoelectron spectroscopy (XPS) were employed to check that no reprecipitation of secondary phases occurred and that the mineral surfaces remained those of a monazite. Coupled with speciation calculations, measured solution compositions permitted the determination of $NdPO_4$ and $GdPO_4$ solubility products which are in general agreement with previous experimental determination on rhabdophane at 25°C, but showing that monazite is more than two orders of magnitude less soluble than inferred on the basis of previous thermodynamic estimates. The temperature evolution from 21 to 300°C of the equilibrium constant (K) of the $NdPO_4$ monazite end-member dissolution reaction given by:

$$NdPO_{4(s)} \leftrightarrows Nd^{3+} + PO_4^{3-}$$

can be described by the equation:

$$-\log K = 7.621 + 0.04163T + 1785/T$$

where T is in Kelvins. Integration of this expression permitted the determination of the enthalpy, free energy and entropy of dissolution and formation of the $NdPO_4$ monazite end-member.

Solubility-speciation calculations show that the presence of aqueous ligands, notably fluoride, carbonate or hydroxide in water strongly affect monazite solubility, depending on pH and temperature. These calculations also show that monazite will exhibit retrograde solubility only under acidic conditions from 70°C to 300°C and to a lesser extent in neutral aqueous solutions from 150°C to 300°C. Solubility-speciation calculations performed on natural seafloor vent hydrothermal fluids and on thermal springwaters from granitic areas at aquifer temperature show that these fluids are equilibrated with respect to monazite. Thus, our study suggests that monazite may play an active role on the control of REE concentrations in crustal waters. Finally, results of this experimental study suggest that a monazite-like nuclear waste form stored underground will show extremely low solubility when in contact with water, especially with granite-equilibrated groundwater. These results therefore confirm the excellent suitability of monazite as a nuclear ceramic. *Copyright © 2004 Elsevier Ltd*

1. INTRODUCTION

Monazite, a monoclinic light rare earth and thorium orthophosphate with the general formula (Ce, La, Nd, Th)PO_4, is currently the subject of considerable interest through its use in geochronology, geothermometry, and more generally in magmatic, metamorphic, and hydrothermal alteration studies (see recent review in Poitrasson et al., 2002). Notably, this mineral is one of the main repositories for light rare earth elements (LREE) in the continental crust (Gavrilova and Turanskaya, 1958; Ward et al., 1992; Bea, 1996), and it has been, and remains one of the main ore minerals of the lanthanides (Smith et al., 1999). It is likely, therefore, that this mineral will play a key role on the control of REE concentrations in crustal waters.

Unfortunately, except for a couple of preliminary studies carried out at high pressure and temperature using a piston-cylinder apparatus (i.e., from 0.2 to 1.8 GPa and from 450°C to 1100°C, Ayers and Watson, 1991; Devidal et al., 1998), no experimental determination of the aqueous solubility of this phase has been reported to date. The only experimental data on rare earth phosphate minerals have been obtained at low temperature on rhabdophane, a hydrous, hexagonal lanthanide phosphate with the general formula $LREEPO_4.xH_2O$ (Tananaev and Vasil'eva, 1963; Jonasson et al., 1985; Firsching and Brune, 1991; Liu and Byrne, 1997). Consequently, predicted monazite solubilities are based on the experimental results obtained on rhabdophane or are calculated from the thermodynamic properties of the constituent oxides (Ousoubalyev et al., 1975; Marinova and Yaglov, 1976; Vieillard and Tardy, 1984; Wood and Williams-Jones, 1994).

We have thus undertaken an experimental solubility study of synthetic $NdPO_4$ and $GdPO_4$ monazite end-members. On the basis of aqueous speciation calculations performed using an updated aqueous REE database, based largely on the work of Haas et al. (1995), the control of monazite on the lanthanide contents of seafloor vent hydrothermal fluids and of thermal granitic springwaters is explored. The suitability of a monazite-

* Author to whom correspondence should be addressed (Franck.Poitrasson@1mtg.obs-mip.fr).

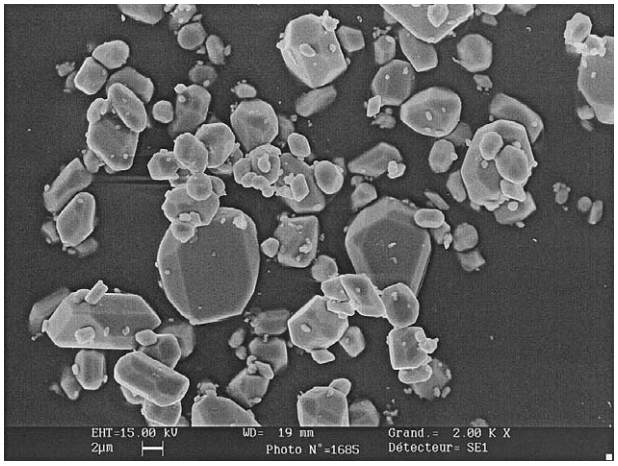

Fig. 1. Scanning electron microscope image, in the secondary electron mode, of the monazite $NdPO_4$ starting material.

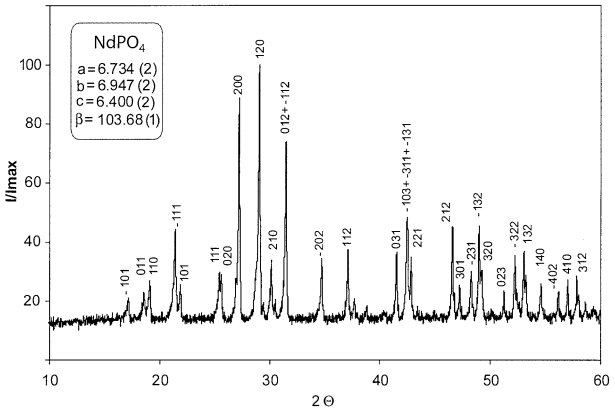

Fig. 2. X-ray diffraction pattern of starting monazite $NdPO_4$, Cu Kα radiation. Lattice parameters in Å except for β in degrees.

like nuclear waste form is then assessed in light of these new results.

2. METHODS

2.1. Monazite Synthesis

Pure $NdPO_4$ monazite end-member crystals were synthesized by flux-assisted crystallization of a $NdPO_4$ gel. The gel is obtained by dissolving neodymium nitrate in water, followed by the addition of an $(NH_4)_2HPO_4$ solution in stoichiometric proportion for a Nd/P 1/1 ratio. This provokes precipitation of a pink gel. The solution is evaporated by boiling, and the precipitate is allowed to dry for a several days. The precipitate is subsequently heated briefly to above 600°C to eliminate NH_4 and nitrates. The final product at this stage is a dry, pink $NdPO_4$ powder. For monazite synthesis, 10 g of this powder was mixed with 5 g of Li_2MoO_4 and 4.2 g of MoO_3 (the flux), in a Pt crucible. The powder and flux mixture is left to react in air at 800°C for 24 h. After cooling, the flux is dissolved in boiling water, and ~5 g of fine pink powder of $NdPO_4$ monazite crystals are recovered. Scanning Electron Microscopy (SEM) aided by Energy Dispersive X-ray spectroscopy (EDX) observation (Fig. 1) confirms that the powder consists of perfectly crystallized crystals, mostly 5–20 μm in size, although smaller crystals are also present. The X-ray diffraction (XRD) pattern (Fig. 2) confirms these crystals are $NdPO_4$ monazite end-member. No other detectable crystalline phases were found. Unit-cell parameters were determined by Fullprof Rieltveld refinement program working in the profile-matching mode. These parameters are a = 6.734(2) Å, b = 6.947(2) Å, c = 6.400(2) Å, and β = 103.68(1)°, which are identical to those obtained by Ni et al. (1995) in a single-crystal study.

The $GdPO_4$ monazite end-member sample was synthesized following a similar procedure. X-ray diffraction patterns and SEM pictures also show that this sample is well crystallized with crystal-sizes similar to those obtained for $NdPO_4$. Nevertheless, this latter phase was chosen for the bulk of our experimental effort since, owing to the intermediate position of Nd among the LREE, it represents a good approximation of natural monazite solid-solution.

2.2. Experimental Protocol

Solubility experiments at 21 ± 1.5°C and 70 ± 1°C were performed in 250 mL polypropylene Nalgene bottles. For room temperature experiments, the bottles were inserted on a rotating support operating continuously. The experiments at 70°C were performed in a thermostated oven and the bottles were regularly shaken manually. Pure titanium (UT 40) reactors placed in continuously rocking heating jackets were used for the experiments performed at 200 ± 1.5°C and 300 ± 1.5°C at saturated vapor pressure. This type of reactor is identical to those used during previous solubility studies (e.g., Castet et al., 1993; Deberdt et al., 1998; Pokrovski and Schott, 1998). The bottles and the titanium reactors were carefully cleaned before the experiments. For the latter, this involved re-machining, followed by cleaning using soap, distilled water and finally 0.1M HNO_3 of the internal reactor walls. This nitric acid cleaning step, performed at 200°C for 2–3 d, also passivated the titanium reactor walls. For all runs, a bi-distilled HCl solution diluted with ultrapure Milli-Q water to obtain a pH = 2 at the experimental temperature was added to the reactors without monazite. This pH was chosen because it avoids formation of carbonates and results in a relatively simple aqueous phosphorous ($H_3PO_{4(aq)}$ and $H_2PO_4^-$) and neodymium (Nd^{3+}) speciation. Furthermore, it yields a rather low ionic strength, close to 0.01 mol/L for all the experiments, which eases activity coefficient determinations. Another incentive for choosing HCl solutions for this study is that association constants for neodymium chloride complexes have been determined experimentally to 250–300°C (Gammons et al., 1996; Stepanchikova and Kolonin, 1999; Migdisov and Williams-Jones, 2002), and they generally show a good agreement with the values computed by Haas et al. (1995), apart from a few exception at the highest temperatures, as discussed below.

After approximately one week at the required temperature, the solutions were sampled to check experimental and sample treatment blank values. These are reported in Table 1 as day "0," and were not subtracted to the samples taken during the experimental runs. Eight hundred milligrams (700 mg for the 300°C experiment) of synthetic monazite was then added to the remaining solution, which measured ~200 mL. For the experiments at high temperature, the reactors were opened and the monazite powder was added to 200 mL of a new solution. This yielded for all experiments an initial solution/solid weight ratio of 250, except for the 300°C experiment for which this ratio was 286. Taking a median grain size of 12.5 μm, a molar weight of 239.21 g/mol and a molar volume of 43.80 cm^3/mol for $NdPO_4$ computed from XRD data (Fig. 2), a powder surface area of 705 cm^2 is estimated using the spherical approximation. With 200 cm^3 of solution, this gives a surface area to volume (S/V) ratio of 3.53 cm^{-1} at the beginning of each experiment.

Solution sampling was carried out at regular intervals to monitor reaction progress. For the low temperature experiments, a polyethylene syringe was used to sample 10 mL of the solution at a time. After filtration of this solution using a Sartorius Minisart polyethylene 0.45 μm filter adaptable to the syringe tip, 5 mL was used for pH measurement and 5 mL was kept for cation and phosphorous analysis by ICP-MS. For the experiments performed in Ti reactors, solution sampling was made through a 2 μm titanium frit mounted in the reactor cover, then subsequently filtered through a water-cooled cell using a 0.45 μm Sartorius cellulose nitrate membrane. This cell was directly attached to the reactor during sampling. Before the experiments, all reagents, recipient and filters were checked for their cleanliness owing to the low level of concentrations encountered in the course of this study.

Table 1. $NdPO_4$ and $GdPO_4$ monazite end-members dissolution experiment results and corresponding solubility products expressed as pKs° (=−log Ks) at zero ionic strength.

Starting material	Temperature							Average ± ISD
$NdPO_4$	Time (days)	0	56	69	90	131	296	
21°C	pH (21°C)	2.03	2.02	2.05	2.03	2.04	2.02	
	P (μM/kg)	0.04	90.7	85.9	91.7	90.4	90.7	
	Nd (μM/kg)	<0.0001	2.70	2.50	2.61	2.43	2.32	
	P/Nd (molar)	nc	33.6	34.4	35.0	37.1	39.1	
	$\log(a_{PO_4^{3-}})$	nc	−19.97	−19.92	−19.94	−19.82	−19.97	
	$\log(a_{Nd^{3+}})$	nc	−5.98	−6.00	−5.99	−6.00	−6.05	
	pKs°	nc	25.95	25.92	25.93	25.82	26.01	25.93 ± 0.07
$NdPO_4$	Time (days)	0	56	69	90	131	296	
70°C	pH (21°C)	2.03	1.99	2.04	2.00	2.04	1.93	
	P (μM/kg)	0.05	75.9	74.3	78.8	79.8	89.1	
	Nd (μM/kg)	<0.0001	0.219	0.200	0.200	0.189	0.194	
	P/Nd (molar)	nc	347	371	392	422	459	
	$\log(a_{PO_4^{3-}})$	nc	−20.01	−19.89	−19.97	−19.86	−20.11	
	$\log(a_{Nd^{3+}})$	nc	−7.13	−7.15	−7.16	−7.18	−7.21	
	pKs°	nc	27.14	27.03	27.14	27.03	27.32	27.13 ± 0.12
$NdPO_4$	Time (days)	0	43	56	77	118	283	
200°C	pH (21°C)	1.97	1.98	2.03	2.00	2.03	1.98	
	P (μM/kg)	0.16	69.1	67.2	65.9	13.8	3.42	
	Nd (μM/kg)	nm	0.00579	0.00575	0.00568	0.0296	0.121	
	P/Nd (molar)	nc	11900	11700	11600	465	28.4	
	$\log(a_{PO_4^{3-}})$	nc	−21.75	−21.61	−21.71	−22.30	−23.05	
	$\log(a_{Nd^{3+}})$	nc	−9.16	−9.12	−9.16	−8.41	−7.85	
	pKs°	nc	30.91	30.74	30.86	30.72	30.90	30.83 ± 0.09
$NdPO_4$	Time (days)	0	43	56	77	118	283	
300°C	pH (21°C)	nm	1.92	1.97	1.95	1.98	1.92	
	P (μM/kg)	0.51	21.4	21.5	22.6	8.07	4.46	
	Nd (μM/kg)	0.0002	0.0216	0.0408	0.0517	0.469	0.894	
	P/Nd (molar)	nc	990	528	437	17.2	4.97	
	$\log(a_{PO_4^{3-}})$	nc	−26.03	−25.91	−25.95	−26.11	−26.41	
	$\log(a_{Nd^{3+}})$	nc	−9.96	−9.63	−9.55	−8.56	−8.34	
	pKs°	nc	35.99	35.54	35.49	34.67	34.75	34.7
$GdPO_4$	Time (days)	0	56	69	90	131	296	
21°C	pH (21°C)	2.03	1.99	2.03	2.01	2.05	1.99	
	P (μM/kg)	0.09	19.7	20.3	20.8	21.5	23.2	
	Gd (μM/kg)	<0.0001	13.4	13.7	14.4	15.2	16.6	
	P/Gd (molar)	nc	1.47	1.47	1.45	1.42	1.40	
	$\log(a_{PO_4^{3-}})$	nc	−20.71	−20.59	−20.63	−20.52	−20.64	
	$\log(a_{Gd}^{3+})$	nc	−5.30	−5.27	−5.26	−5.22	−5.21	
	pKs°	nc	26.01	25.86	25.89	25.74	25.84	25.87 ± 0.10

nc: not calculated; nm: not measured. No standard deviation is given for the 300°C experiment since the selected pKs° figure stems from the last two, stable samples taken 118 and 283 days after the start of the experiment.

2.3. Potentiometric, Analytical and Spectroscopic Methods

pH measurements were performed at room temperature (21 ± 1.5°C) immediately after sampling using a glass Schott-Geräte H62 electrode and a Philips PW9422 digital pH-meter. The solution was continuously stirred with a magnetic stirrer. The electrode was calibrated using NBS/DIN $pH_{21°C} = 4.001$, $pH_{21°C} = 6.881$ and $pH_{21°C} = 9.26$ buffer solutions. Regression coefficients (r) better than 0.9999 were obtained and our pH measurements are thought to be precise to within 0.02 pH units. Accordingly, repeated pH measurements of solutions sampled from room temperature experiments show variations not much larger than this (Table 1), and these incorporate other sources of potential experimental variations.

Neodymium, gadolinium, and phosphorous analyses were performed by Inductively Coupled Plasma-Mass Spectrometry (ICP-MS) on 5-mL samples that were acidified to 0.32 mol/L HNO_3 and 10^{-4} mol/L HF using bi-distilled acids, and into which In and Re internal standards were added. This sample preparation was carried out within 24 h of sampling to minimize the effects of evaporation or reprecipitation during sample storage. This led to a total dilution factor of ~2. The analyses were conducted at the end of the experimental runs, to minimize potential accuracy problems that may arise for very low concentrations if ICP-MS calibrations of different days were used for different samples from a given experimental run. The Perkin-Elmer Elan 6000 ICP-MS was calibrated using commercial standard solutions at four different dilutions. Phosphorous is difficult to analyze at the ppb (part per billions) level by most commonly used techniques, including ICP-MS. For the latter, this results from the poor ionization potential of this element, coupled with $^{15}N^{16}O$ and $^{14}N^{16}OH$ interferences at the unique mass 31 of phosphorous. We thus used a modified desolvation system for these analyses which reduced significantly the oxide and hydroxides interferences, thus permitting the quantitative determination of phosphorous at concentrations down to at least a few hundred ppt (part per trillions). This was verified using 0.5, 5, 50 and 1000 ppb standard solutions. The resulting calibration curves exhibited an excellent linearity with regression coefficients (r) better than 0.9999. Accuracy for P and the cations was checked against synthetic and natural standard solutions and is estimated to be better than 10%. Precisions are estimated to be better than 5% (1RSD).

Table 2. Azero parameters used in the speciation calculation performed in this study (see text for sources).

Azero (Å)	Species
3	$NdCl_{3(aq)}$, $NdF_{3(aq)}$, $Nd(OH)_{3(aq)}$, $H_3PO_{4(aq)}$, NO_3^-, Cl^-.
4	$NdCl_2^+$, $NdCl_4^-$, NdF_2^+, NdF_4^-, $Nd(OH)_2^+$, $Nd(OH)_4^-$, $NdCO_3^+$, $NdSO_4^+$, $H_2PO_4^-$, HPO_4^{2-}, PO_4^{3-}, SO_4^{2-}, F^-.
4.5	$NdCl^{2+}$, NdF^{2+}, $NdOH^{2+}$, $NdNO_3^{2+}$, $NdHCO_3^{2+}$, $NdPO_{4(aq)}$, $Nd(PO_4)_2^{3-}$, $NdHPO_4^+$, $Nd(HPO_4)_2^-$, $NdH_2PO_4^{2+}$.
5	Nd^{3+}, CO_3^{2-}.
9	H^+.

After all experiments, the solids were recovered and dried to 110°C overnight in an oven. The crystal surfaces were studied with a LEO/435VP scanning electron microscope used mostly in the secondary electron mode. The operating conditions involved an acceleration voltage of 15 kV, a working distance of 19 mm and a probe current of ca. 1.5 nA. Relative chemical analysis of the mineral surfaces were obtained by X-ray Photoelectron Spectroscopy (XPS) using a VG Escalab MkII operated with a Al Kα excitation source. A deconvolution of an X-ray photoelectron spectrum can in principle yield the chemical environment of the elements occurring near the solid surfaces. In the present case, this is not possible as nothing is known about Nd or Gd XPS spectra in a monazite structure. Nevertheless, changes in the peak shapes after the experiments would indicate a modification of the chemical environment of these elements on the mineral surfaces, even if they cannot be identified. More importantly, relative abundance of the elements can be calculated by peak integration after application of sensitivity factors. These elemental ratios are considered to be accurate to within 10%.

2.4. Speciation Calculations

Speciation calculations were performed using the EQ3NR code (Wolery, 1992) to estimate the activity of aqueous species and compute solubility products at zero ionic strength. The standard state adopted for the aqueous species other than H_2O is unit activity in a hypothetical one molal solution referenced to infinite dilution at any temperature and pressure. For minerals and H_2O, the standard state corresponds to unit activity of the pure phase at any temperature and pressure. Activity coefficient γ_i of the i^{th} charged species was calculated according to the B-dot equation of Helgeson (1969):

$$\log \gamma_i = -\frac{A_\gamma Z_i^2 \sqrt{I}}{1 + \mathring{a}_i^2 B_\gamma \sqrt{I}} + \mathring{B} I \quad (1)$$

where I is the ionic strength of the solution defined as

$$I = \frac{1}{2} \sum_i M_i Z_i^2 \quad (2)$$

M_i being the molality of the i^{th} element and Z_i its charge; A_γ and B_γ are characteristic parameters of the solvent; $\mathring{B}$ ("B-dot") is a corrective factor for this extended Debye-Hückel equation and $\mathring{a}_i$ is the "effective diameter" of the i^{th} ion in solution (listed in Table 2). These parameters were mostly taken from a modified version of the EQ3NR database.

Thermodynamic properties of rare earth aqueous species were calculated using association constants from Lee and Byrne (1992), Millero (1992) and Haas et al. (1995). The latter reference gives parameters which enabled calculation of association constants to 300°C at saturated vapor pressure using the SUPCRT92 code (Johnson et al., 1992). Values of association constants for aqueous Nd species and phosphoric acid used in our calculations are reported in Table 3. The experiments on which these association constants are based were mostly carried out at 25°C. However, experimental studies of neodymium chloride complexation from 25 to 300°C (Gammons et al., 1996; Stepanchikova and Kolonin, 1999; Migdisov and Williams-Jones, 2002) found association

Table 3. Stability constants at zero ionic strength and saturated vapor pressure used in the speciation calculation performed in this study (see text for sources).

Reaction	LogK 0.01°C	25°C	60°C	100°C	150°C	200°C	250°C	300°C
$Nd^{3+} + Cl^- \leftrightarrows NdCl^{2+}$	0.13	0.31	0.65	1.08	1.65	2.28	2.98	3.84
$Nd^{3+} + 2Cl^- \leftrightarrows NdCl_2^+$	−0.23	0.03	0.48	1.06	1.83	2.71	3.75	5.10
$Nd^{3+} + 3Cl^- \leftrightarrows NdCl_{3(aq)}$	−0.53	−0.32	−0.01	0.38	0.95	1.67	2.66	4.13
$Nd^{3+} + 4Cl^- \leftrightarrows NdCl_4^-$	−0.74	−0.74	−0.85	−0.99	−1.12	−1.08	−0.75	0.07
$Nd^{3+} + F^- \leftrightarrows NdF^{2+}$	4.06	4.37	4.85	5.41	6.12	6.85	7.66	8.60
$Nd^{3+} + 2F^- \leftrightarrows NdF_2^+$	7.42	7.56	7.89	8.35	9.02	9.82	10.8	12.1
$Nd^{3+} + 3F^- \leftrightarrows NdF_{3(aq)}$	10.1	9.88	9.79	9.81	10.0	10.5	11.3	12.6
$Nd^{3+} + 4F^- \leftrightarrows NdF_4^-$	12.6	11.8	10.9	10.0	9.18	8.66	8.55	9.06
$Nd^{3+} + H_2O \leftrightarrows NdOH^{2+} + H^+$	−9.47	−8.13	−6.61	−5.24	−3.92	−2.87	−2.01	−1.28
$Nd^{3+} + 2H_2O \leftrightarrows Nd(OH)_2^+ + 2H^+$	−19.6	−17.1	−14.3	−11.9	−9.56	−7.80	−6.39	−5.19
$Nd^{3+} + 3H_2O \leftrightarrows Nd(OH)_{3(aq)} + 3H^+$	−30.2	−26.4	−22.3	−18.8	−15.7	−13.4	−11.7	−10.3
$Nd^{3+} + 4H_2O \leftrightarrows Nd(OH)_4^- + 4H^+$	−41.6	−37.1	−32.1	−27.7	−23.7	−20.7	−18.5	−16.7
$Nd^{3+} + CO_3^{2-} \leftrightarrows NdCO_3^+$	8.05	7.70	7.41	7.24	7.22	7.41	7.84	8.67
$Nd^{3+} + HCO_3^- \leftrightarrows NdHCO_3^{2+}$	1.77	1.85	2.10	2.48	3.03	3.65	4.36	5.22
$Nd^{3+} + NO_3^- \leftrightarrows NdNO_3^{2+}$	1.30	0.79	0.35	0.09	−0.03	0.04	0.27	0.70
$Nd^{3+} + PO_4^{3-} \leftrightarrows NdPO_{4(aq)}$	11.8	11.8	11.8	11.8	11.8	11.8	11.8	11.8
$Nd^{3+} + 2PO_4^{3-} \leftrightarrows Nd(PO_4)_2^{3-}$	19.5	19.5	19.5	19.5	19.5	19.5	19.5	19.5
$Nd^{3+} + HPO_4^{2-} \leftrightarrows NdHPO_4^+$	5.18	5.18	5.18	5.18	5.18	5.18	5.18	5.18
$Nd^{3+} + 2HPO_4^{2-} \leftrightarrows Nd(HPO_4)_2^-$	8.66	8.66	8.66	8.66	8.66	8.66	8.66	8.66
$Nd^{3+} + H_2PO_4^- \leftrightarrows NdH_2PO_4^{2+}$	2.57	2.31	2.18	2.22	2.43	2.78	3.26	3.93
$Nd^{3+} + SO_4^{2-} \leftrightarrows NdSO_4^+$	3.37	3.64	4.06	4.53	5.14	5.81	6.64	7.77
$PO_4^{3-} + H^+ \leftrightarrows HPO_4^{2-}$	12.60	12.32	12.12	12.08	12.18	12.43	12.82	13.39
$HPO_4^{2-} + H^+ \leftrightarrows H_2PO_4^-$	7.323	7.205	7.189	7.288	7.526	7.867	8.319	8.936
$H_2PO_4^- + H^+ \leftrightarrows H_3PO_{4(aq)}$	2.070	2.170	2.354	2.593	2.917	3.276	3.698	4.257
$2H_3PO_{4(aq)} \leftrightarrows H_4P_2O_{7(aq)} + H_2O$	6.18	6.55	7.13	7.95	9.33	11.3	14.2	19.4

constants mostly within one log unit of the values extrapolated by Haas et al. (1995), thus validating experimentally these calculated constants. In detail, it appears neodymium chloride association constants determined by Gammons et al. (1996) and Migdisov and Williams-Jones (2002) tend to show stronger complexation than the Haas et al. (1995) figures suggest at the highest temperature. This is not confirmed by the experimental determinations of Stepanchikova and Kolonin (1999), however, which show close agreement with Haas et al. (1995) values from 150 to 250°C. On the other hand, Wood et al. (2002) made experiments leading to increasingly smaller neodymium hydroxide association constants as temperature increases than Haas et al. (1995) estimates, suggesting that hydroxides complex less easily with neodymium at higher temperatures than previously thought. We nevertheless kept the Haas et al. (1995) values, largely based on the low temperature figures of Lee and Byrne (1992) and Millero (1992), for the sake of internal database consistency, since most neodymium association constants with other important ligands such as fluoride, carbonate or phosphate were not determined experimentally yet. Further, the experimental chloride and hydroxide associations constants were generally not determined at regular temperature intervals and some species were not investigated. The effect of the contrasted association constants recently determined by certain authors at higher temperatures will nevertheless be assessed below.

Since the pH of sampled solutions were measured at room temperature, even for the higher temperature experiments, we adopted a two-step procedure for speciation calculations at elevated temperature. The first step involved a calculation at 21°C using the measured pH and adjusting Cl^- to achieve electroneutrality. The Cl^- value found was then used in a second speciation calculation, again with EQ3NR, to determine the pH at elevated temperature.

3. RESULTS

3.1. Dissolution Behavior and Stoichiometry

The temporal evolution of the reactive solution constituent compositions are listed for all experiments in Table 1 and illustrated in Figure 3. Stable concentrations for P, Nd and Gd are reached in less than two months for experiments at 21 and 70°C. Molar P/cation ratios tend to be higher than one (Fig. 4), contrarily to what should be expected from stoichiometric dissolution. For instance, the 21°C $NdPO_4$ experiment has an aqueous P/Nd ratio of between 30 and 40. With an estimated surface area to solution volume ratio of 3.53 cm^{-1}, the measured aqueous Nd and P concentrations correspond to dissolution of surface layers of 3 and 110 Å of the mineral grains, respectively, assuming that this process occurs homogeneously. Taking into account the size of a $NdPO_4$ monazite end-member unit cell (see Ni et al., 1995 and Fig. 2), this suggests that the Nd present in solution stems from the leaching of one atomic layer, whereas P would require the leaching of more than thirty layers, thus resulting in an altered surface. However, formation of such a thick altered surface seems unlikely from a crystal chemical point of view. Accordingly, XPS measurements show that the P/Nd ratio of the solids phases remains close to one after the experiment made at 21°C (Table 4). As XPS gives the chemical composition of the first few atomic layers of a mineral surface, these spectroscopic measurements therefore rule out this altered layer scenario. This deviation from the stoichiometric aqueous P/Nd ratio cannot be explained by reprecipitation of a Nd-rich and P-poor phase on the mineral surface either since neither the XPS measurements (Table 4) nor the SEM observations (Fig. 5) support this. Hence, the most likely scenario is that the starting products, despite several steps of cleaning, were not completely pure and contained excess of phosphorous, perhaps in the form of inclusions close to the mineral surfaces. For the experiment with $NdPO_4$ at 21°C, this can be explained by the occurrence of ~0.6 mg of pure phosphorous in the starting material. This is only less than 0.1% of the 800 mg of monazite powder used in the experiment and seems therefore possible.

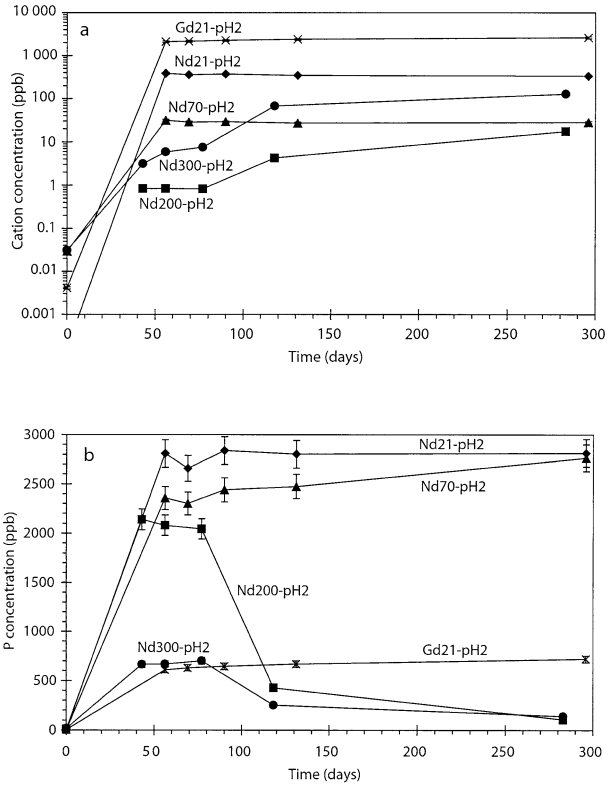

Fig. 3. Neodymium and gadolinium concentrations (a) and phosphorous concentration (b) as a function of time showing the evolution of these element contents in the experimental solutions. Note the logarithm scale of Figure 3a.

A good argument for the above hypothesis is the observation that the experiment with $GdPO_4$ at 21°C yielded a P/cation ratio much closer to stoichiometry (Fig. 4) without any apparent reason in terms of dissolution mechanisms. To check this, some of the $NdPO_4$ monazite recovered after the first run was subjected to an additional 2 months experiment at 21°C and pH = 2 with a new solution. The aqueous P/Nd molar ratio was 1.3 for the additional experiment, very close to the expected stoichiometric dissolution. The occurrence of an excess of phosphorous in some of our starting materials does not affect calculated solubility products however, because both phosphorous and the cation were analyzed. Nevertheless, these results show that assuming a stoichiometric dissolution and analyzing cations only (Liu and Byrne, 1997) can lead to significant computational errors.

Aqueous concentrations varied more significantly for the 200°C and 300°C experiments (Table 1; Fig. 3). A temporal decrease of the aqueous P/Nd ratio towards the stoichiometric value is observed over the ca. nine months of experiment (Fig. 4). Such high-temperature experiments were repeated and this behavior appears to be reproducible. XPS analyses of the

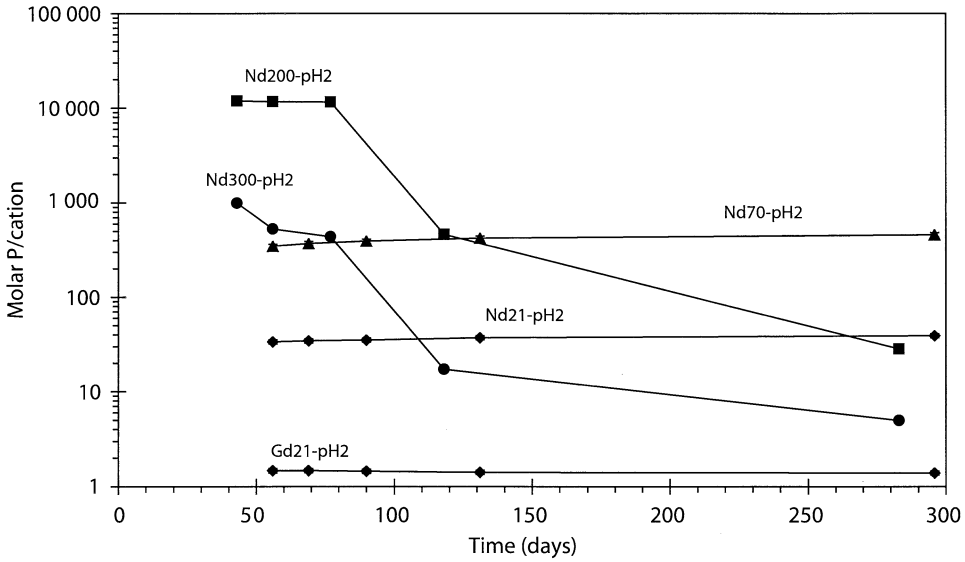

Fig. 4. Molar P/Nd or P/Gd through time showing the stoichiometry of the dissolution during the various experiments.

mineral surfaces reacted at 300°C show that the P/Nd ratio remained similar to that of the starting material grain surfaces (Table 4), and SEM observations did not show any reprecipitations on these surfaces (Fig. 5b). These P and Nd atoms released in solution at high temperature represent a small amount of the initial monazite (ca. 0.01%). It is thus feasible that the high temperature experimental conditions allowed for a kinetically enhanced chemical equilibration between the bulk monazite and the solution, through ion diffusion in the solid. Constant total ion activities observed from 21°C to 200°C during the experiments (Table 1) show that equilibrium solubility products were obtained in less than two months. At 300°C, stable solubility products are obtained later, after 3 months. But at the higher temperatures (200°C and 300°C), ionic diffusion in the solid becomes fast enough to allow a progressive re-equilibration between the whole monazite and the solution. If the experiments would have lasted for longer than one year, one would expect the solution to reach the whole monazite stoichiometric P/Nd ratio of one. Whatever the exact mechanism of this P/Nd ratio reequilibration observed during the high temperature experiments, this did not affect significantly the calculated solubility products, as they remain essentially constant from 43 to 283 d after the start of the 200°C experiments, and for the last 165 days of the 300°C experiment (Table 1).

3.2. Aqueous Speciation in Experimental Solutions

Results of speciation calculations, summarized in Table 5, indicate that the free cation is the dominant REE aqueous species and that phosphorous is mostly present as $H_3PO_{4(aq)}$ and $H_2PO_4^-$ at low temperature, as shown by previous studies (e.g., Jonasson et al., 1985; Liu and Byrne, 1997). At higher temperature, chloride and hydroxide species become significant for the cation, and at 300°C $NdCl^{2+}$ is by far the dominant aqueous Nd species. For phosphorous, $H_3PO_{4(aq)}$ dominates with increasing temperature to 200°C. Finally, aqueous $H_4P_2O_{7(aq)}$ becomes significant above 200°C. These calculations show that the speciation becomes increasingly complicated with temperature, in accordance with the lowering of the water dielectric constant. This observation has implications for the Nd and P concentrations in equilibrium with monazite in natural waters at elevated temperatures, as discussed below.

3.3. Solubility Products

The logarithm of the aqueous activities of Nd^{3+}, Gd^{3+} and PO_4^{3-} were calculated with the EQ3NR code using the procedure described above and are reported in Table 1. For the dissolution of, for example, $NdPO_4$, expressed by

Table 4. X-ray photoelectron spectroscopy measurements on starting material and after some experiments.

	$NdPO_4$ before experiment		$NdPO_4$, 21°C experiment		$NdPO_4$, 300°C experiment	
Element (electronic shell)	Peak centre (eV)	Atomic ratio	Peak centre (eV)	Atomic ratio	Peak centre (eV)	Atomic ratio
Nd (4d)	131.8	1	132.2	1	132.9	1
P (2p)	142.5	0.95	143.3	0.99	143.6	0.97
O (1s)	540.5	4.40	541.4	4.07	541.7	3.99
C (1s)	294.0	4.21	295.2	2.55	295.8	2.46

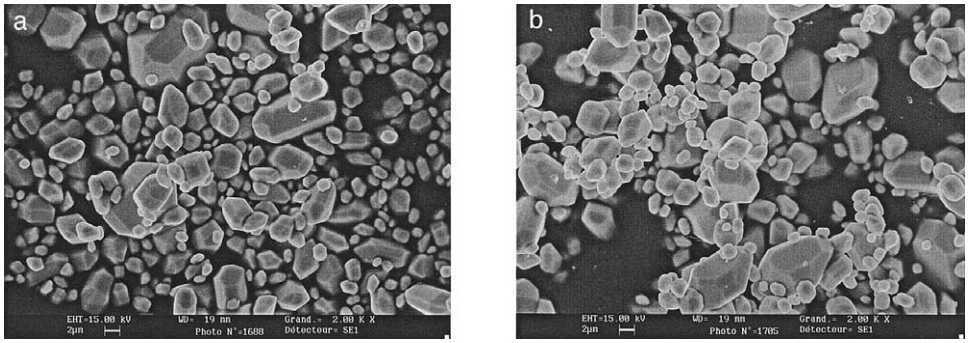

Fig. 5. Scanning electron microscope images, in the secondary electron mode, of the monazite $NdPO_4$ after experimental runs at 21°C (a) and 300°C (b).

$$NdPO_{4(s)} \leftrightarrows Nd^{3+} + PO_4^{3-} \quad (3)$$

the logarithm of the solubility product at zero ionic strength (pKs°) can be calculated with

$$pKs^\circ = -\log(a_{Nd^{3+}}) - \log(a_{PO_4^{3-}}) \quad (4)$$

where a_i stands for the activity of the subscripted aqueous species. Values of these pKs° are reported in Table 1 for each sampled reactive solution. If a significant trend could be observed with time, this could suggest that a phase other than monazite may also have played a role in controlling aqueous Nd or P concentrations. In agreement with XPS and SEM observations, this does not appear to be the case; pKs° values are essentially found to be time-independent. These stable pKs° enabled estimation of the precisions associated with these solubility product determinations. They are on the order of ± 0.1 log units for all temperatures (Table 1). The only exception to this is the 300°C experiment which appears to have reached a stable pKs° later, between 90 and 131 days after the start of the experiment. These uncertainties notably include the precision on pH measurements, ICP-MS analyses, sample handling and storage before analysis. On the other hand, the accuracy of these pKs° determinations will be primarily limited by the accuracy of the association constant used in the speciation calculations. As discussed above, the largest discrepancies between the association constant computed by Haas et al. (1995) and some recent experimental determinations occur at the highest temperatures (cf. Gammons et al., 1996, 2002; Wood et al., 2002). To evaluate the impact of these new associations constants on the calculated pKs, we have done additional speciation calculations for our experiment is at 300°C which are the most likely to be influenced by different Cl and OH association constants given the importance of Nd hydroxide and chloride complexes at such temperature (Table 5). Using association constants of Gammons et al. (1996) and Wood et al. (2002) at 300°C instead of those of Haas et al. (1995) minimizes $NdOH^{2+}$ compared to the Nd-chloride species and increases our pKs° by less than 0.9 log units. Hence, conservative estimates of the uncertainties of our pKs°, taking into account uncertainties on association constants, may range from a few tens of log units at 25°C, up to a log unit at 300°C. The observation that measured pKs° values are time independent indicates that the variation in stoichiometry observed during dissolution at elevated temperatures had little effect, if any, on the final solubility products. It is apparent from Table 1 that monazite shows a decreasing solubility product (Ks) with increasing temperature, as previously inferred on the basis of calculated negative enthalpies of dissolution of rare earth phosphates (Marinova and Yaglov, 1976).

Table 5. Speciation of the experimental solutions calculated with EQ3NR.

Temperature (°C)	21	70	200	300
Neodymium species (%)				
Nd^{3+}	98.5	96.4	53.0	4.7
$NdCl^{2+}$	1.05	3.38	43.1	80.9
$NdOH^{2+}$	«1	«1	3.15	8.38
$NdCl_2^+$	«1	«1	«1	5.97
Phosphorous species (%)				
$H_3PO_{4(aq)}$	55.0	72.7	94.1	22.8
$H_2PO_4^-$	45.0	27.3	5.93	«1
$H_4P_2O_{7(aq)}$	«1	«1	«1	77.1

To our knowledge, these are the first published experimentally determined monazite aqueous solubility products. We can therefore only compare these results with the thermodynamic estimates of Vieillard and Tardy (1984), which themselves are based on thermodynamic calculations of Ousoubalyev et al. (1975) and Tananaev and Petrushkova (1967). They expressed $NdPO_4$ dissolution as:

$$NdPO_{4(s)} + 2H^+ \leftrightarrows Nd^{3+} + H_2PO_4^- \quad (5)$$

and reported −log K values for this reaction of 2.87 and 2.77, respectively. Recalculating these constants for reaction (3) using the phosphate protonation constants given in Table 3 yields pKs° of 23.40 and 23.30, respectively. This is more than two orders of magnitude lower than the experimentally determined pKs° of 25.93 for $NdPO_4$ obtained in the present study (Table 1). Our experiments therefore show that monazite is less soluble than previously thought. Similar conclusions apply for $GdPO_4$.

Previous experimental REE-phosphate solubility studies were performed on rhabdophane, a hydrous hexagonal LREE phosphate ($LREEPO_4.xH_2O$). The pKs° of $NdPO_4.xH_2O$ at 25°C was found to be 25.91 (Jonasson et al., 1985), 25.95 (Firsching and Brune, 1991) and 26.20 (Liu and Byrne, 1997), which are closely consistent with the −log Ks of $NdPO_4$

monazite end-member obtained in the present study (Table 1). Similarly, our pKs° of 25.87 for $GdPO_4$ monazite end-member (Table 1) is close to the Gd-rhabdophane reported values of 25.39 of Firshing and Brune (1991) and 25.62 of Liu and Byrne (1997), and to a lesser extent to the figure of 24.82 of Tananaev and Petushkova, (1967; recalculated at zero ionic strength by Byrne and Kim, 1993).

Comparison of X-ray photoelectron analyses of the mineral surfaces before and after the experiments shows that $NdPO_4$ was not transformed as $NdPO_4.xH_2O$ since the O/Nd ratio did not increase (Table 4), as would have been required if this transformation occurred. Furthermore, the XPS O(1s) spectra remain unchanged, which is an other indication that oxygen of the mineral surfaces remained in the same structural environment after the experiment, thereby ruling out the appearance of hydrated rhabdophane. This confirms that the solubility products determined in our experiments (Table 1) are those of monazite. Hence, the similarity between $NdPO_4$ and $NdPO_4.xH_2O$ solubility products at ca. 25°C and atmospheric pressure suggests that we are close to the thermodynamic conditions where both phases are stable, as illustrated by Langmuir and Melchior (1985) on gypsum and anhydrite around 56°C. Accordingly, Carron et al. (1958) have shown that monazite is stable and can precipitate in aqueous solutions under 100°C provided that enough time is given for the reaction to occur. Further evidence for the low-temperature stability of monazite is that it is found in detrital sediments resulting from igneous rock weathering (i.e., stream sediments and beaches), and it forms as a weathering product of REE-rich minerals (Rose et al., 1958; Meintzer and Mitchell, 1988).

At higher temperatures, we can only compare our data with monazite solubility calculation performed by Wood and Williams-Jones (1994). They also expressed $NdPO_4$ dissolution using Eqn. 5 and gave $-\log K$ values for this reaction of 8.01 and 10.94 at 200°C and 300°C, respectively. Recalculating these constants for Eqn. 3 using the phosphorous protonation constants given in Table 3 yields pKs° values of 28.31 and 33.27 at 200°C and 300°C, respectively. These values are again ~2 log units lower than those obtained experimentally in this study (Table 1). This discrepancy likely stems from extrapolative uncertainties associated with the Wood and Williams-Jones (1994) high temperature monazite solubility estimates, which were based on thermodynamic parameters obtained at 25°C, themselves leading to too low monazite solubility estimates at low temperature as shown above.

3.4. Derivation of Thermodynamic Quantities for $NdPO_4$

It is apparent in Figure 6 that $-\log K$ (i.e., pKs°) of $NdPO_4$ is not a linear function of the reciprocal temperature, and therefore, the heat capacity of the dissolution is not equal to zero. A fit of these data can be obtained by first considering the van't Hoff relation given by:

$$\frac{\partial \ln K}{\partial (1/T)} = -\frac{\Delta H^\circ}{R} \tag{6}$$

and the definition of isobaric heat capacity (ΔCp°):

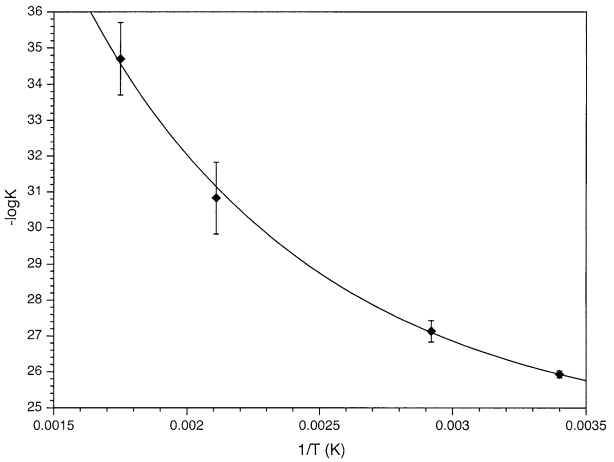

Fig. 6. Evolution of $NdPO_4$ solubility product at zero ionic strength, expressed as pKs°, as a function of the reciprocal temperature. The curve is the best fit (r=0.9992) of the experimental points using Eqn. 13. The uncertainties used for the regression, taking into account inaccuracies in association constant knowledge are 0.1 log unit at 21°C, 0.3 log units at 70°C and 1 log unit at 200°C and 300°C. See text for details.

$$\left[\frac{\partial \Delta H^\circ}{\partial T}\right]_p = \Delta Cp^\circ \tag{7}$$

in which ln K is the natural logarithm of the equilibrium constant K, ΔH° is the standard enthalpy change of the reaction, R is the gas constant and T the absolute temperature in Kelvins. Assuming the temperature variation of ΔCp° can be described using the classical empirical Maier and Kelly (1932) equation given by:

$$\Delta Cp^\circ = a + bT + c/T^2 \tag{8}$$

where a, b and c are adjustable parameters, this Eqn. 8 can be combined with an integrated form of expression (7) to yield:

$$\Delta H^\circ = aT + bT^2/2 - c/T + Ct_1 \tag{9}$$

where Ct_1 is an integration constant. Combining Eqn. 6 and (9) and integrating leads to:

$$\ln K = -\frac{Ct_1}{RT} + \frac{a \ln T}{R} + \frac{bT}{2R} + \frac{c}{2RT^2} + Ct_2 \tag{10}$$

where Ct_2 is an other integration constant. This equation corresponds to an expression of the general form

$$\log K = A + BT + C/T + D\log T + E/T^2 \tag{11}$$

where A through E are constants, T is absolute temperature in Kelvins and noting that natural logarithms have been replaced by decimal logarithms. Such an expression is often used to fit the temperature variation of solubility products or dissociation constants (Plummer and Busenberg, 1982; Langmuir, 1996). To apply Eqn. 11 to the data obtained at only four unique temperatures and showing a non-linear relationship with the reciprocal of the temperature (Fig. 6), a three parameter model is sufficient. This was done by fixing parameters D and E to 0 to obtain:

Table 6. Thermodynamic quantities for $NdPO_4$ monazite end-member at 298.15K calculated from the experimental results obtained in this study.

	$\Delta G°_s$ (kJ/mol)	$\Delta H°_s$ (kJ/mol)	$\Delta S°_s$ (J/mol/K)
$NdPO_4$	**148.5**	**−34.7**	**−621**
	$\Delta G°_f$ (kJ/mol)	$\Delta H°_f$ (kJ/mol)	$S°_f$ (J/mol/K)
Nd^{3+} [a]	−672.0	−696.6	
PO_4^{3-} [a]	−1019	−1277	
$NdPO_4$	**−1839.5**	**−1937**	**178** [b]
$NdPO_4$ [c]	−1824	−1930	167
$NdPO_4$ [d]	−1816	−1941	116
$NdPO_4$ [e]		−1932	137
$NdPO_4$ [f]		−1968	

s and f subscripts stand for solubility and formation, respectively. Sources: [a]: SUPCRT92 database (Johnson et al., 1992); [b] Calculated with entropies ($S°_{298.15K}$) of Nd, P and O_2 taken from Robie et al. (1978); [c]: from Ousoubalyev et al. (1975); [d]: from Marinova and Yaglov (1976); [e]: from Wood and Williams-Jones (1994); [f]: from Ushakov et al. (2001). Values in bold were calculated from this study (see text).

$$\log K = A + BT + C/T \quad (12)$$

which is a simplified form of the expression used by Plummer and Busenberg (1982) to fit carbonate solubilities. Result of the fit of Eqn. 12 to the $NdPO_4$ monazite end-member solubility data obtained in the present study is:

$$-\log K = 7.621 + 0.04163T + 1785/T \quad (13)$$

This Eqn. 13 can be used to recalculate pKs° of $NdPO_4$ at any temperature between 21 and 300°C. Combined with the appropriate classical thermodynamic expressions, it can be used to calculate at any temperature (between 21 and 300°C in the present case) the variations for reaction (3) in Gibbs free energy ($\Delta G°_s$), enthalpy ($\Delta H°_s$) and entropy ($\Delta S°_s$), where "s" stands for solubility, using the formalism of Plummer and Busenberg (1982). These thermodynamic quantities at 298.15K were calculated and are reported in Table 6. Using these values and the $\Delta G°_f$ and $\Delta H°_f$ of aqueous Nd^{3+} and PO_4^{3-}, where "f" stands for "formation," taken from the SUPCRT92 database, it was then possible to estimate $\Delta G°_f$, $\Delta H°_f$ and $S°_f$ of $NdPO_4$ monazite end-member, also reported in Table 6.

The $\Delta H°_f$ value derived from the present experiments compares well (Table 6) with corresponding calculated values reported by Marinova and Yaglov (1976), Ousoubalyev et al. (1975) and Wood and Williams-Jones (1994). However, all these figures are less negative than recent calorimetric measurements of Ushakov et al. (2001). On the other hand, the $\Delta G°_f$ and $S°_f$ generated above (Table 6) are closer to the estimates of Ousoubalyev et al. (1975) than those of Marinova and Yaglov (1976). It should be emphasized that the $\Delta G°_f$ value of Marinova and Yaglov (1976) is the one chosen in the compilations of Vieillard and Tardy (1984) and then by Wood and Williams-Jones (1994). Our $GdPO_4$ experiments at 21°C enable us to compute a $\Delta G°_s$ and $\Delta G°_f$ of 145.7 kJ/mol and −1828 kJ/mol, respectively, although the latter is not strictly comparable to the −1816 kJ/mol value of Marinova and Yaglov (1976) and Ousoublalyev et al. (1975) because they gave it at a slightly higher temperature of 25°C. Further experimental work is required to determine these thermodynamic quantities for all the REE phosphate series.

4. GEOCHEMICAL APPLICATIONS

4.1. REE Control in Hydrothermal Fluids by Monazite

These solubility results (Table 1) show that monazite in equilibrium with pure water will lead to the lowest REE concentration compared to other simple REE-bearing solid phases such as carbonates, fluorides and hydroxides (Firsching and Mohammadzadel, 1986; Menon et al., 1987; Deberdt et al., 1998). Hence, monazite is likely to play a key role on the control of REE concentrations in crustal fluids, although ligands present in natural aqueous fluids may affect monazite dissolution. This possibility is assessed below with the aid of speciation calculations performed using EQ3NR on theoretical solutions as well as on some natural fluids taken from case studies.

4.1.1. Theoretical considerations

Results of $NdPO_4$ monazite end-member solubility-speciation calculations over the temperature range 10–300°C at acidic, neutral and alkaline pH are illustrated in Figure 7. These acidic, neutral and basic solutions were controlled in the calculations to have pH values of pH_{n-3}, pH_n and pH_{n+3} respectively, where pH_n refers to the pH of neutrality at any temperature (Table 7). Taking account of natural solutions (Baas Becking et al., 1960), the Eh of these acidic, neutral and basic solutions were taken to be 0.5, 0.2 and 0 V, respectively. To compare the effect of aqueous ligands on REE speciation, carbonate, fluoride, chloride, sulfate and nitrate concentrations were set equal to 0.003 molal. Sodium and calcium were selected as cations, which were adjusted for charge balance during the calculations. This led to solutions with a ionic strength ~0.01 mol/L. Finally, neodymium and phosphate concentrations were constrained by the monazite solubility determined in this study, assuming stoichiometric dissolution. The results in Figure 7 are plotted in terms of absolute concentrations of aqueous Nd species.

An important result from these calculations is that although monazite displays a decreasing solubility product (Ks = −log pKs; Fig. 6) with increasing temperature, total neodymium concentration in the model solution decreases with increasing temperature at acidic conditions only above 60°C (Fig. 7a), from ca. 160 ppb to ~2 ppb, and at neutral conditions only above 150°C (Fig. 7b). In contrast, at basic conditions, $NdPO_4$ monazite end-member solubility is prograde (Fig. 7c). This latter result illustrates the influence of aqueous complexation on solubility. Whereas the concentration of aqueous Nd^{3+} decreases by nearly ten orders of magnitude between 10 and 300°C, the total Nd concentration actually increases by more than four orders of magnitude (Fig. 7c), from ca. 0.2 ppb to over 500 ppb.

The degree to which each ligand contributes to monazite solubility depends on temperature and pH. Our calculation of theoretical fluids with equal ligand concentrations show that under acidic conditions, fluoride complexes dominate, with

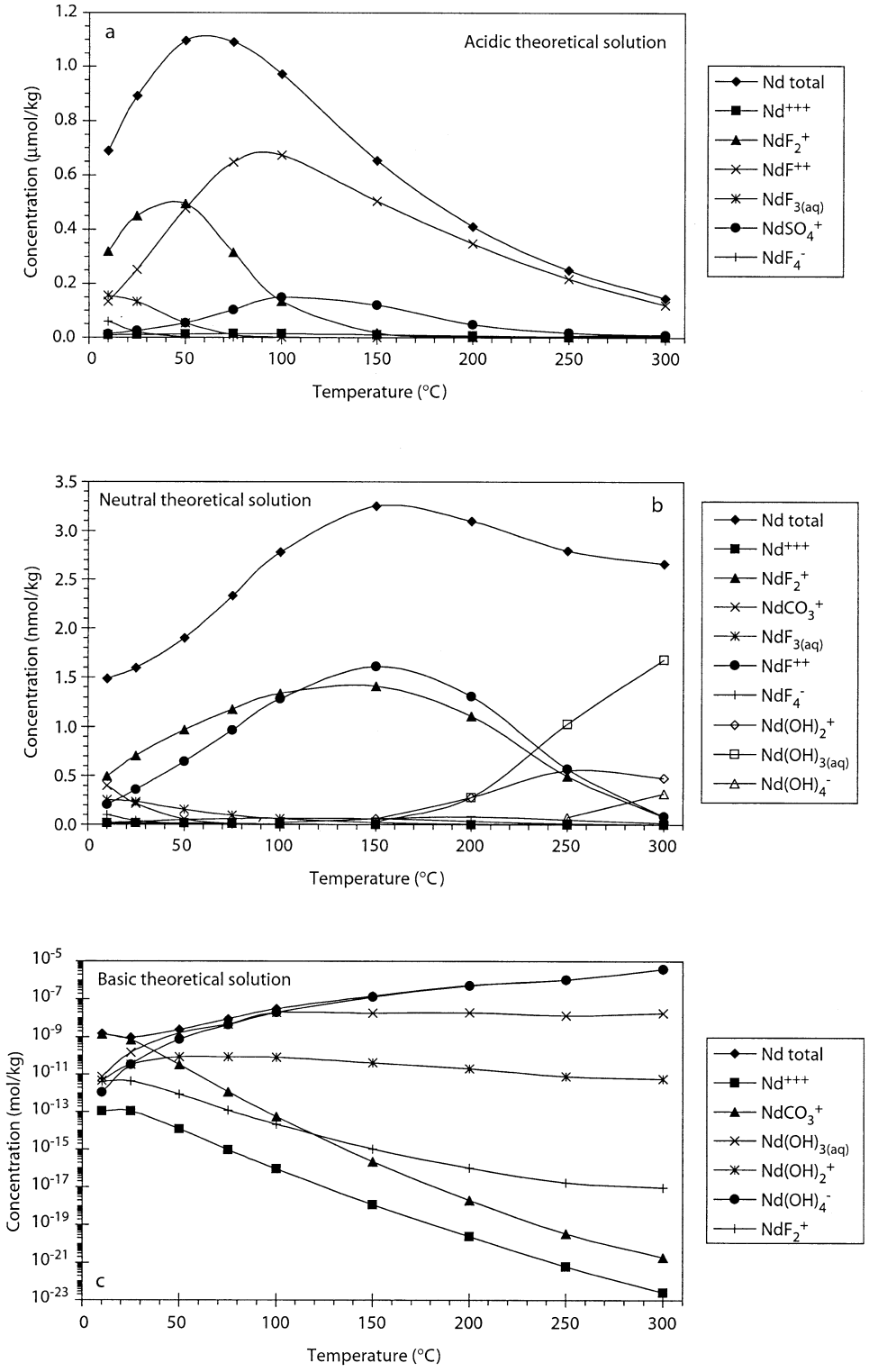

Fig. 7. Results of $NdPO_4$ solubility-speciation calculations for acidic (a), neutral (b) and basic (c) theoretical solutions at various temperatures. Note the different units for each figure, and the logarithm scale for (c). See Table 7 and text for details and discussion.

tendency for complexes having fewer fluoride ions per neodymium cations to become more stable as temperature increases (Fig. 7a). Neodymium-sulfate complexes are the second most abundant species after fluorides, but they never exceed 15% of the total speciation. At neutral conditions, solute speciation is more complex. Although NdF_2^+ and NdF^{2+} dominate over

Table 7. pH used for monazite solubility-speciation calculations on theoretical solutions (based on water dissociation constants of Sweeton et al., 1974).

Temperature (°C)	Acidic pH	Neutral pH	Basic pH
10	4.28	7.28*	10.28
25	4.00	7.00	10.00
50	3.64	6.64	9.64
75	3.35	6.35	9.35
100	3.13	6.13	9.13
150	2.82	5.82	8.82
200	2.65	5.65	8.65
250	2.60	5.60	8.60
300	2.65	5.65	8.65

* : Linearly interpolated value

most of the temperature range to 200°C, carbonate complexes are significant at low temperatures and hydroxide species become dominant above 250°C. Nevertheless, total neodymium concentrations ranging from 0.21 ppb at 10°C to 0.47 ppb at 150°C are essentially dictated, as under acidic conditions, by fluoride complexation. At alkaline conditions carbonate complexes dominate from 10 to ~30°C, whereas hydroxide complexes dominate at higher temperatures. Such a predominance of rare earth hydroxide complexes under alkaline conditions for hydrothermal fluids at elevated temperatures was already pointed out by Haas et al. (1995).

As noted above, some experimental studies of Nd chloride and hydroxide complexation (Gammons et al., 1996, 2002; Wood et al., 2002) found an increasing discrepancy with Haas et al. (1995) computed association constants with increasing temperature. To evaluate the effect of these experimentally determined constants on our calculations, these were introduced in our EQ3NR database and the calculations performed again to see the effect in the most critical situation, i.e., at 300°C. Although the experimental determinations at high temperature are not as comprehensive as the Haas et al. (1995) database in terms of species and temperature range, it appears that total Nd concentrations and speciation remain unchanged under basic conditions (pH=8.65 at 300°C, see Table 7), and show negligible differences under acidic medium (i.e., total Nd concentrations and individual species abundances vary by less than 10%). On the other hand, use of the speciation constants of Gammons et al. (1996) and Wood et al. (2002) for neutral conditions (pH=5.65 at 300°C, Table 7) leads to a total Nd concentration lower by a factor of two and makes neodymium fluoride species more abundant than hydroxides, as calculated with Haas et al. (1995) constants for lower temperatures (Fig. 7).

Comparing concentrations at constant temperature as a function of pH shows that at 25°C, Nd total concentrations decrease as pH increases (Fig. 7). In contrast, at 150°C and 300°C, the lowest concentrations are observed at neutral conditions, although the highest Nd concentration occurs at acidic conditions at 150°C whereas the highest concentration at 300°C is observed in alkaline solutions.

To summarize, it appears that for a solution having equal ligand concentrations, only fluoride, hydroxide, and at low temperature, carbonate ions play a significant role on monazite solubility.

4.1.2. *Natural case studies*

Because of very low concentrations, reliable REE analyses of crustal hydrothermal fluids became available only in the late 1980s (Michard and Albarède, 1986; Michard, 1989). Phosphorous analyses of these waters are still rare for the same reason. Nevertheless, measurement of these elements is essential to assess the role of monazite on aqueous lanthanide concentrations in hydrothermal fluids, phosphorous being probably controlled by more abundant phosphate minerals such as apatite. The calculations performed in the present study were made with an aim to better understand seafloor hydrothermal vent fluid composition reported by Wood and Williams-Jones (1994) and the thermal granitic springwaters analyzed by van Middlesworth and Wood (1998), for which both REE and phosphorous concentrations were provided. Furthermore, these authors already attempted to assess the role of monazite on the geochemistry of these waters. This will thus be an opportunity to compare their results, based on calculated monazite solubility from thermochemical values of the monazite constituting elements (Wood and Williams-Jones, 1994), with our new calculations based on experimental data and the association constants given in Table 3. It should be noted that for all the calculations, including the values from Wood and Williams-Jones (1994) reported in Table 8 and van Middlesworth and Wood (1998) given in Table 9, we have taken a pure $NdPO_4$ monazite end-member for comparative purposes. The calculated aqueous Nd concentrations should thus be considered as an upper estimate since Nd typically represents 15–20% of the total REE content of monazite, although the $NdPO_4$ solubility product determined in this study appears to be close to the partial solubility product of the neodymium end-member of natural monazite (Poitrasson et al., 2000a). Nevertheless, the comparison made below should not be considered much more precise than the order of magnitude level given the uncertainties of speciation calculations at higher temperatures, as discussed above.

4.1.3. *Seafloor hydrothermal vent fluids*

The results of the monazite solubility-speciation calculations for seafloor hydrothermal vent fluids are given in Table 8. Our calculation for the 300°C fluid is in reasonable agreement with the computed speciation and Nd concentration reported by Wood and Williams-Jones (1994), especially when considering the difference of two orders of magnitude in the monazite solubility products taken for these two calculations (see part 3.3 above). This indicates that the effect of the higher monazite solubility used by these authors was cancelled out by weaker association constants compared to those used in the present study and reported Table 3. This fact is illustrated by later calculations performed by Gammons et al. (1996, their Table 7) with similar fluid composition and monazite solubility product, but higher neodymium chloride complex association constants determined experimentally which yield Nd concentrations ~100 times higher than those in Table 8. Taking our monazite solubility determination, Gammons et al. (1996) neodymium chloride association constants, but Wood et al. (2002) neodymium hydroxide association constants (which are weaker than those of Wood and Williams-Jones (1994) and Haas et al.

Table 8. Results of monazite solubility-speciation calculations for seafloor hydrothermal vent fluids (concentrations in mol/kg).

Source:	W&W, 1994[a]	This study	W&W, 1994[a]	This study
Starting fluid:				
T(°C)	300		200	
pH (at temperature)	4.5		4.5	
Na	0.560		0.560	
Ca	0.037		0.037	
Cl	0.600		0.600	
ΣPO_4	3×10^{-7}		3×10^{-7}	
Calculation results:				
$NdOH^{2+}$	6.00×10^{-10}	7.91×10^{-11}	1.08×10^{-9}	1.25×10^{-10}
$NdCl^{2+}$	9.20×10^{-11}	5.07×10^{-11}	6.80×10^{-10}	1.61×10^{-10}
$Nd(OH)_2^+$	nc	2.39×10^{-11}	nc	7.18×10^{-12}
$NdCl_2^+$	nc	1.12×10^{-11}	nc	1.88×10^{-11}
$Nd(OH)_{3(aq)}$	nc	2.37×10^{-12}	nc	2.99×10^{-13}
Nd^{3+}	4.40×10^{-11}	2.27×10^{-12}	2.28×10^{-9}	5.11×10^{-11}
Nd total	7.36×10^{-10}	1.70×10^{-10}	4.04×10^{-9}	3.64×10^{-10}
Nd measured[b]	From 1.4×10^{-10} to 1.0×10^{-8}			

[a] : Wood and Williams-Jones, 1994; nc: not calculated. [b] : Values of Piepgras and Wasserburg, 1985; Michard and Albaréde, 1986; Klinkhammer et al., 1994; Douville et al., 1999.

(1995)) in our EQ3NR database leads to negligible Nd-hydroxide species with respect to chlorides, and to a total Nd concentration of 8.9×10^{-10} mol/kg, i.e., even closer to the original Wood and Williams-Jones (1994) calculated concentration (Table 8). At 200°C, the difference between our calculations and the aqueous Nd concentrations computed by Wood and Williams-Jones (1994) is larger than at 300°C since our total Nd concentration is ten times lower (Table 8). Nevertheless our results still confirm that aqueous Nd concentrations in these fluids will increase with decreasing temperature, though to a lesser extent than predicted by Wood and Williams-Jones (1994). The calculations show that the main lanthanide species present in solution are hydroxides and chlorides. Hence, assuming a priori a negligible role of hydroxide ligands in these hydrothermal fluids because they are mildly acidic (Douville et al., 1999) is clearly misleading if Wood and Williams-Jones (1994) or Haas et al. (1995) association constants are considered (Table 8). Further, the fact that our calculated Nd concentrations are within the lower range of those measured in hydrothermal vent fluids (0.02 to 1.5 ppb, Piepgras and Wasserburg, 1985; Michard and Albarède, 1986; Klinkhammer et al., 1994; Douville et al., 1999) suggests that lanthanide phosphates may play an important role on the control of natural hydrothermal aqueous lanthanide concentrations, at least for those fluids showing lower rare earth contents. It may be argued that the REE patterns of these fluids commonly display a large positive europium anomaly, similar to those of plagioclases from the host rock they interact with (Klinkhammer et al., 1994; Douville et al., 1999). However, it is feasible that at least the trivalent REE released in the hydrothermal fluids by plagioclase and other mineral dissolutions will have an upper concentration limit controlled by monazite reprecipitation.

4.1.4. *Thermal springwaters from granitic areas*

The thermal springwaters used in these illustrative calculations are dilute, neutral to alkaline and $NaHCO_3$-dominated (van Middlesworth and Wood, 1998). Chemical Na-K geothermometers suggest aquifer equilibration temperatures ranging from ~60 to 230°C. Representative sources of these extremes were taken for our calculations. For Horse Creek, an alkaline, low temperature aquifer spring (Table 9), the relative abundance of the Nd-species obtained from speciation calculations is in broad agreement with the calculated values of van Middlesworth and Wood (1998). In contrast, there are huge differences in the computed concentrations: our aqueous Nd concentration at vent temperature is five orders of magnitude lower than that of van Middlesworth and Wood (1998), whereas at aquifer temperature (94°C) our concentration is six order of magnitude lower (Table 9). Likewise for Big Creek, a neutral, hot aquifer spring (Table 9), the relative abundances of species roughly agree, but our concentrations are still lower compared to those calculated by van Middlesworth and Wood (1998), though to a lesser extent. At vent temperatures, our concentration is 300 times lower whereas at aquifer temperature (222°C), it is 100 times lower (Table 9). Clearly, the differences of monazite solubility product can account for two orders of magnitude difference, whereas the remaining can be attributed to the speciation calculations. For instance, our PO_4^{3-} activities are in most cases higher than those of van Middlesworth and Wood (1998), sometimes by more than an order of magnitude (Table 9).

The result is that, making allowance for the uncertainties of speciation calculations, our calculated Nd concentrations at aquifer temperature are within the range of values measured in filtered springwaters, whereas the concentrations calculated at vent temperature are clearly lower (Table 9). On the basis of their calculations, van Middlesworth and Wood (1998) proposed a scenario whereby waters should be undersaturated with respect to monazite in the aquifer and then would become saturated and precipitate monazite during water ascent. In contrast, our results clearly indicate that the waters were equilibrated with monazite in the aquifers, and then became oversaturated while the water rose. This scenario is in much better

Table 9. Results of monazite solubility-speciation calculations for granitic thermal springwaters

	Horse Creek, vent temperature		Horse Creek, aquifer temperature		Big Creek vent temperature		Big Creek, aquifer temperature	
	v&W, 1998[a]	This study	v&W, 1998[a]	This study	v&W, 1998[a]	This study	v&W, 1998[a]	This study
Starting fluid (mg/l)								
Temperature	38.5°C		94°C		93.2°C		222°C	
pH	9.2		9.2		7.16		7.16	
Eh(V)	−0.007		−0.007		−0.32		−0.32	
ΣHCO_3^-	69.4		69.4		481		481	
F	6.7		6.7		15.3		15.3	
CL	2.1		2.1		27.6		27.6	
ΣPO_4^{3-}	0.08		0.08		0.05		0.05	
ΣSO_4^{2-}	4.81		4.81		48.1		48.1	
$SiO_{2(aq)}$	92.8		92.8		91.3		91.3	
Li	0.16		0.16		0.95		0.95	
Na	40.6		40.6		214		214	
K	0.6		0.6		22.7		22.7	
Ca	2.53		2.53		5.11		5.11	
Sr	na		na		0.23		0.23	
Ba	0.1		0.1		0.17		0.17	
Ni	0.64		0.64		1.97		1.97	
Hg	0.35		0.35		0.44		0.44	
Pb	0.04		0.04		0.08		0.08	
Calculations results: Major anion activities (mol/kg)								
Cl^-	5.61×10^{-5}	5.57×10^{-5}	5.54×10^{-5}	5.53×10^{-5}	6.86×10^{-4}	6.92×10^{-4}	6.53×10^{-4}	6.50×10^{-4}
F^-	3.34×10^{-4}	3.32×10^{-4}	3.30×10^{-4}	3.29×10^{-4}	7.11×10^{-4}	7.18×10^{-4}	6.69×10^{-4}	6.75×10^{-4}
SO_4^{2-}	3.91×10^{-5}	3.84×10^{-5}	3.63×10^{-5}	3.73×10^{-5}	2.47×10^{-4}	5.04×10^{-6}	1.28×10^{-6}	2.39×10^{-4}
HCO_3^-	8.62×10^{-4}	9.50×10^{-4}	6.85×10^{-4}	1.01×10^{-3}	6.83×10^{-3}	6.14×10^{-3}	3.91×10^{-3}	4.92×10^{-3}
CO_3^{2-}	8.09×10^{-5}	8.92×10^{-5}	7.74×10^{-5}	2.99×10^{-5}	7.07×10^{-6}	7.30×10^{-6}	5.75×10^{-7}	7.94×10^{-6}
$H_2PO_4^-$	6.98×10^{-10}	5.66×10^{-9}	7.16×10^{-10}	3.03×10^{-8}	1.08×10^{-6}	2.15×10^{-7}	4.59×10^{-7}	2.23×10^{-7}
HPO_4^{2-}	7.33×10^{-8}	5.90×10^{-7}	5.60×10^{-8}	5.89×10^{-7}	7.80×10^{-7}	1.68×10^{-7}	5.45×10^{-8}	1.35×10^{-7}
PO_4^{3-}	6.71×10^{-11}	5.59×10^{-10}	6.97×10^{-11}	1.78×10^{-10}	8.82×10^{-12}	2.03×10^{-12}	2.03×10^{-13}	2.39×10^{-12}
Calculation results: Neodymium species concentrations (mol/kg)								
$NdCO_3^+$	6.10×10^{-10}	4.05×10^{-14}	—	—	6.31×10^{-12}	3.05×10^{-14}	—	—
$Nd(OH)_{3(aq)}$	4.23×10^{-9}	1.05×10^{-14}	3.38×10^{-6}	5.43×10^{-12}	2.01×10^{-11}	2.76×10^{-14}	1.49×10^{-7}	$1.04 \times 10^{10^{-9}}$
$NdPO_{4(aq)}$	—	3.89×10^{-15}	—	—	—	—	—	—
$Nd(OH)_2^+$	5.34×10^{-10}	3.82×10^{-15}	—	2.01×10^{-13}	1.25×10^{-11}	2.79×10^{-14}	—	—
$Nd(OH)_4^-$	7.63×10^{-10}	8.26×10^{-16}	1.08×10^{-5}	1.96×10^{-12}	—	—	7.01×10^{-7}	7.10×10^{-9}
$NdOH^{2+}$	—	7.48×10^{-16}	—	—	3.67×10^{-12}	1.65×10^{-14}	—	—
NdF^{2+}	—	—	—	—	9.01×10^{-12}	4.85×10^{-14}	—	—
NdF_2^+	—	—	—	—	5.27×10^{-12}	2.23×10^{-14}	—	—
Nd^{3+}	—	—	—	—	—	5.71×10^{-16}	—	—
Nd total	6.17×10^{-9}	6.07×10^{-14}	1.41×10^{-5}	7.60×10^{-12}	5.75×10^{-11}	1.76×10^{-13}	8.49×10^{-7}	8.14×10^{-9}
Measured Nd	4.16×10^{-10}				4.23×10^{-10}			

[a] van Middlesworth and Wood, 1998; na: not analyzed; -: below 2.5% of the total Nd concentration (v&W, 1998) or below 1% of the total Nd concentration (this study). Measured water composition for major elements and Nd are from v&W, 1998.

agreement with the residence time of the waters in their aquifers estimated to be in the range of 9000 to 40000 years (Young, 1985). This time is certainly long enough to reach thermodynamic equilibrium, even for monazite (Oelkers and Poitrasson, 2002). Petrology also supports the equilibration of deep hot waters with monazite, since primary magmatic allanite from the host granites has been reported to be hydrothermally altered to monazite (Wood and Ricketts, 2000).

The lanthanide concentrations measured by van Middlesworth and Wood (1998) on springwaters from Idaho are similar to concentrations previously found on comparable waters from granitic areas elsewhere in the world (typically between 6 and 110 ppt, Michard and Albarède, 1986; Michard et al., 1987; Möller et al., 1998; Négrel et al., 2000). It is thus likely that the scenario proposed here is widely applicable.

4.2. Implications for Nuclear Ceramics

Natural monazite interactions with fluids result in varied alteration mechanisms (Poitrasson et al., 1996; 2000b). Among these, total dissolution was illustrated to be among the significant processes occurring in the degradation of this mineral. The results obtained in the present study may therefore help to assess the behavior of monazite-like nuclear waste forms (e.g., Boatner and Sales, 1988) in underground storage facilities.

The calculations reported in paragraph 4.1.4. above clearly show that a repository located in a granitic area is likely to be safe with regard to a monazite nuclear-waste form even if water percolates, as long as this water keeps its natural composition. The calculated Nd concentrations resulting from monazite dissolution at aquifer temperatures range from one ppt at 94°C to

one ppb at the highest temperature 222°C (Table 9). At lower temperatures, the calculated concentrations remain at the low ppq (part per quadrillions) level, implying that monazite dissolution will be extremely restricted.

In the event that engineered barriers will affect the composition of the interacting waters, the calculation performed on theoretical fluids may be of some guidance (see part 4.1.1. above and Fig. 7). For instance, these results show that the repository should be designed to avoid the release of fluorine ions if a monazite-like matrix is to be used. Accordingly, this is the ligand which will enhance most significantly monazite solubility at equal ligand concentrations under neutral, and especially acidic conditions (Fig. 7a and b). It is also well known that leaching concrete leads initially to very alkaline waters (Neal, 1996), and such waters will enhance monazite dissolution at elevated temperatures (Fig. 7c). Nevertheless, even in the most severe theoretical cases shown in Figure 7, such as pH = 3.64 at 50°C with 0.003 mol/L F^- or pH = 8.65 at 300°C (equivalent to pH = 10 at 25°C, see Table 7), the amount of Nd released by monazite dissolution remains below the ppm level. Taking 1 ppm and assuming complete equilibration between monazite and water to make a conservative estimate, fluid/mineral ratios in excess of 60 000 are required to dissolve only 10% of a monazite nuclear ceramic. Accordingly, it is unlikely that such a ratio will be approached while keeping a fluid with the extreme conditions described above and a fluid flow rate low enough to reach equilibrium at all times. All this therefore confirms that monazite is an excellent matrix for the underground storage of high level nuclear wastes as far as matrix-water interactions are concerned.

Acknowledgments—This manuscript reports parts of a long-term study during which the first author benefited from discussions with many individuals, including Fabrice Brunet, Sylvie Castet, Simon Chenery, Nicolas Dacheux, Jean-Louis Dandurand, Samuel Deberdt, Gleb Pokrovsky and Jon Robinson. Gilles Berger is especially thanked for providing his PowerMacintosh compiled version of EQ3NR and SUPCRT92 and for numerous clarifications on the topic. The experimental part benefited a lot from the help and presence of Jean Claude Harrichoury. Thanks should also go to Remi Freydier and Michel Valladon for making this mighty desolvation system for ICP-MS analysis working properly at last. Djar Ochab is acknowledged for his patience behind the SEM and Gérard Chatainier for his expert help in XPS determination. Thanks to Jean Luc Devidal, LMV Clermont-Ferrand for X-Ray diffraction, and to Daniel Avignant for initiating Jean Marc Montel to Rietveld refinement. Dave Wesolowski and two anonymous referees are acknowledged for their insightful reviews. Scott Wood's particularly fair review was much appreciated. This work was financed by CNRS and ANDRA through the GdR FORPRO (research action number 98.c) and corresponds to the GdR FORPRO contribution number 2001/05 A.

Associate editor: D. J. Wesolowski

REFERENCES

Ayers J. C. and Watson E. B. (1991) Solubility of apatite, monazite, zircon and rutile in supercritical aqueous fluids with implications for subduction zone geochemistry. *Phil. Tran. R. Soc. London* **A335,** 365–375.

Baas Becking L. G. M., Kaplan I. R., and Moore D. (1960) Limits of the natural environment in terms of pH and oxidation-reduction potentials. *J. Geol.* **68,** 243–284.

Bea F. (1996) Residence of REE, Y, Th and U in granites and crustal protoliths; Implications for the chemistry of crustal melts. *J. Petrol.* **37,** 521–552.

Boatner L. A. and Sales B. C. (1988) Monazite. In *Radioactive waste forms for the future* (eds. W. Lutze and R. C. Ewing), pp. 495–564. North-Holland.

Byrne R. H. and Kim K. H. (1993) Rare earth precipitation and coprecipitation behavior: The limiting role of PO_4^{3-} on dissolved rare earth concentrations in seawater. *Geochim. Cosmochim. Acta* **57,** 519–526.

Carron M. K., Naeser C. R., Rose H. J., and Hildebrand F. A. (1958) Fractional precipitation of rare earths with phosphoric acid. *USGS Bull.* **1036-N,** 253–275.

Castet S., Dandurand J. L., Schott J., and Gout R. (1993) Boehmite solubility and aqueous aluminium speciation in hydrothermal solutions (90–350°C). Experimental study and modeling. *Geochim. Cosmochim. Acta* **57,** 4869–4884.

Deberdt S., Castet S., Dandurand J. L., Harrichoury J. C., and Louiset I. (1998) Experimental study of $La(OH)_3$ solubilities (25 to 150°C), and La-acetate complexing (25 to 80°C). *Chem. Geol.* **151,** 349–372.

Devidal J. L., Gibert F., Kieffer B., Pin C., and Montel J. M. (1998) A new method for solubility measurement: application to $NdPO_4$ system in H_2O-NaCl-HCl hydrothermal fluids. *Mineral. Mag.* **62A,** 375–376.

Douville E., Bienvenu P., Charlou J. L., Donval J. P., Fouquet Y., Appriou P., and Gamo T. (1999) Yttrium and rare earth elements in fluids from various deep-sea hydrothermal systems. *Geochim. Cosmochim. Acta* **63,** 627–643.

Firsching H. F. and Brune S. N. (1991) Solubility products of the trivalent rare earth phosphates. *J. Chem. Eng. Data* **36,** 93–95.

Firsching H. F. and Mohammadzadel J. (1986) Solubility products of the rare earth carbonates. *J. Chem. Eng. Data* **31,** 40–42.

Gammons C. H., Wood S. A., and Williams-Jones A. E. (1996) The aqueous geochemistry of the rare earth elements and yttrium: VI. Stability of neodymium chloride complexes from 25 to 300°C. *Geochim. Cosmochim. Acta* **60,** 4615–4630.

Gammons C. H., Wood S. A. and Li Y. (2002) Complexation of the rare earth elements with aqueous chloride at 200°C and 300°C and saturated water vapor pressure. In *Water-rock interactions, ore deposits and environmental geochemistry: A tribute to David A. Crerar*. (ed. R. Hellmann and S. A. Wood), Vol. 7, pp. 191–207. The Geochemical Society.

Gavrilova L. K. and Turanskaya R. V. (1958) Distribution of rare earth in rock-forming and accessory minerals of certain granites. *Geochem.* **2,** 163–170.

Haas J. R., Shock E. L., and Sassani D. C. (1995) Rare earth element in hydrothermal systems: Estimates of standard partial molal thermodynamic properties of aqueous complexes of the rare earth elements at high pressures and temperatures. *Geochim. Cosmochim. Acta* **59,** 4329–4350.

Helgeson H. C. (1969) Thermodynamics of hydrothermal systems at elevated temperatures and pressures. *Am. J. Sci.* **267,** 729–804.

Johnson J. W., Oelkers E. H., and Helgeson H. C. (1992) SUPCRT92: A software package for calculating the standard molal properties of minerals, gases, aqueous species and reactions among them from 1 to 5000 bars and 0 to 1000°C. *Comp. Geosci.* **18,** 899–947.

Jonasson R. G., Bancroft G. M., and Nesbitt H. W. (1985) Solubilities of some hydrous REE phosphates with implications for diagenesis and sea water concentrations. *Geochim. Cosmochim. Acta* **49,** 2133–2139.

Klinkhammer G. P., Elderfield H., Edmond J. M., and Mitra A. (1994) Geochemical implications of rare earth elements patterns in hydrothermal fluids from mid-ocean ridges. *Geochim. Cosmochim. Acta* **58,** 5105–5113.

Langmuir D. (1996) Aqueous environmental geochemistry. Prentice-Hall.

Langmuir D. and Melchior D. (1985) The geochemistry of Ca, Sr, Ba and Ra sulfates in some deep brines from the Palo Duro Basin, Texas. *Geochim. Cosmochim. Acta* **49,** 2423–2432.

Lee J. H. and Byrne R. H. (1992) Examination of comparative rare earth element complexation behavior using linear free-energy relationships. *Geochim. Cosmochim. Acta* **56,** 1127–1137.

Liu X. and Byrne R. H. (1997) Rare earth and yttrium phosphate solubilities in aqueous solution. *Geochim. Cosmochim. Acta* **61,** 1625–1633.

Maier C. G. and Kelly K. K. (1932) An equation for the representation of high temperature heat content data. *J. Am. Chem. Soc.* **54,** 3243–3246.

Marinova L. A. and Yaglov V. N. (1976) Thermodynamic characteristics of lanthanide phosphates. *Russian J. Phys. Chem.* **50,** 477.

Meintzer R. E. and Mitchell R. S. (1988) The epigene alteration of allanite. *Can. Mineral.* **26,** 945–955.

Menon M. P., James J., and Jackson J. D. (1987) Studies on the solubility and complexation of lanthanum and neodymium fluoride-water systems. *Lanthan. Actin. Res.* **2,** 49–66.

Michard A. (1989) Rare earth element systematics in hydrothermal fluids. *Geochim. Cosmochim. Acta* **53,** 745–750.

Michard A. and Albarède F. (1986) The REE content of some hydrothermal fluids. *Chem. Geol.* **55,** 51–60.

Michard A., Beaucaire C., and Michard G. (1987) Uranium and rare earth elements in CO_2-rich waters from Vals-les-Bains (France). *Geochim. Cosmochim. Acta* **51,** 901–909.

Migdisov A. A. and Williams-Jones A. E. (2002) A spectrophotometric study of neodymium(III) complexation in chloride solutions. *Geochim. Cosmochim. Acta* **66,** 4311–4323.

Millero F. J. (1992) Stability constants for the formation of rare earth inorganic complexes as a function of ionic strength. *Geochim. Cosmochim. Acta* **56,** 3123–3132.

Möller P., Dulski P., Gerstenberger H., Morteani G., and Fuganti A. (1998) Rare earth elements, yttrium and H, O, C, Sr, Nd and Pb isotope studies in mineral waters and corresponding rocks from NW-Bohemia, Czech Republic. *Appl. Geochem.* **13,** 975–994.

Neal F. B. (1996) Modelling the long-term chemical evolution of cement-groundwater systems. In *Scientific basis for nuclear waste management XIX* **Vol. 412** (eds. W. M. Murphy and D. A. Knecht), pp. 483–490. Material Research Society.

Négrel P., Guerrot C., Cocherie A., Azaroual M., Brach M., and Fouillac C. (2000) Rare earth elements, neodymium and strontium isotopic systematics in mineral waters: evidence from the Massif Central, France. *Appl. Geochem.* **15,** 1345–1367.

Ni Y., Hughes J. M., and Mariano A. N. (1995) Crystal chemistry of the monazite and xenotime structures. *Am. Mineral.* **80,** 21–26.

Oelkers E. H. and Poitrasson F. (2002) An experimental study of the dissolution stoichiometry and rates of natural monazite as a function of temperature from 50 to 230°C and pH from 1.5 to 10. *Chem. Geol.* **191,** 73–87.

Ousoubalyev I, Batkybekova M, Yousoupov V, Kydynov M (1975) Les propriétés thermochimiques des phosphates et des iodates des éléments des terres rares. *4e Conférence Internationale de Thermodynamique Chimique*. 217–223.

Piepgras D. J. and Wasserburg G. J. (1985) Strontium and neodymium isotopes in hot springs on the East Pacific Rise and Guyamas basin. *Earth Planet. Sci. Lett.* **72,** 341–356.

Plummer L. N. and Busenberg E. (1982) The solubilities of calcite, aragonite and vaterite in CO_2-H_2O solutions between 0 and 90°C, and an evaluation of the aqueous model for the system $CaCO_3$-CO_2-H_2O. *Geochim. Cosmochim. Acta* **46,** 1011–1040.

Poitrasson F., Chenery S., and Bland D. J. (1996) Contrasted monazite hydrothermal alteration mechanisms and their geochemical implications. *Earth Planet. Sci. Lett.* **145,** 79–96.

Poitrasson F., Oelkers E. H., Schott J., and Montel J. M. (2000a) Experimental study of monazite-water interaction from 21 to 300°C. *Goldschmidt Conference, Oxford, J. Conf. Abstr.* **5,** 805–806.

Poitrasson F., Chenery S., and Shepherd T. J. (2000b) Electron microprobe and LA-ICP-MS study of monazite hydrothermal alteration: Implications for U-Th-Pb geochronology and nuclear ceramics. *Geochim. Cosmochim. Acta* **64,** 3283–3297.

Poitrasson F., Hanchar J. M., and Schaltegger U. (2002) The current state and future of accessory mineral research. *Chem. Geol.* **191,** 3–24.

Pokrovski G. and Schott J. (1998) Thermodynamic properties of aqueous Ge(IV) hydroxide complexes from 25 to 350°C: Implications for the behavior of germanium and the Ge/Si ratio in hydrothermal fluids. *Geochim. Cosmochim. Acta* **62,** 1631–1642.

Robie R. A, Hemingway B. S, Fisher J. R (1978) Thermodynamic properties of minerals and related substances at 298.15 K and 1 bar (10^5 Pascals) pressure and at higher temperatures. *Geol. Surv. Bull.* **1452,** 456 pp.

Rose H. J., Blade L. V., and Ross M. (1958) Earthy monazite at Magnet Cove, Arkansas. *Am. Min.* **43,** 995–997.

Smith M. P., Henderson P., and Peishan Z. (1999) Reaction relationships in the Bayan Obo Fe-REE-Nb deposit, Inner Mongolia, China: implications for the relative stability of rare-earth element phosphates and fluorocarbonates. *Contrib. Mineral Petrol.* **134,** 294–310.

Stepanchikova S. A. and Kolonin G. R. (1999) Spectrophotometric study of complexation of neodymium in chloride solutions at temperatures up to 250°C. *Zh. Neorg. Khim.* **44 (***10***),** 1744–1751.

Sweeton F. H., Mesmer R. E., and Baes C. F., Jr. (1974) Acidity measurements at elevated temperatures. VII. Dissociation of water. *J. Sol. Chem.* **3,** 191–214.

Tananaev I. V. and Petushkova S. M. (1967) The reaction of gadolinium chloride with orthophosphate ions in aqueous solution at 25°C. *Russ. J. Inorg. Chem.* **12,** 39–42.

Tananaev I. V. and Vasil'eva V. P. (1963) Lanthanum phosphates. *Russ. J. Inorg. Chem.* **8,** 555–558.

Ushakov S. V., Helean K. B., Navrotsky A., and Boatner L. A. (2001) Thermochemistry of rare-earth orthophosphates. *J. Mat. Res.* **16,** 2623–2633.

van Middlesworth P. E. and Wood S. A. (1998) The aqueous geochemistry of the rare earth elements and yttrium. Part 7. REE, Th and U contents in thermal springs associated with the Idaho batholith. *Appl. Geochem.* **13,** 861–884.

Vieillard P. and Tardy Y. (1984) Thermochemical properties of phosphates. In *Phosphate minerals* (eds. J. O. Nriagu and P. B. Moore), pp. 171–198. Springer-Verlag.

Ward C. D., McArthur J. M., and Walsh J. N. (1992) Rare earth element behaviour during evolution and alteration of the Dartmoor granite, SW England. *J. Petrol.* **33,** 785–815.

Wolery T. J (1992) E3/6, a software package for geochemical modeling of aqueous systems: Package overview and installation guide (ver. 7.0). UCRL-MA-110662 Pt I, Lawrence Livermore National Laboratories.

Wood S. A., Palmer D. A., Wesolowski D. J. and Bénézeth P. (2002) The aqueous geochemistry of the rare earth elements and yttrium. Part XI. The solubility of $Nd(OH)_3$ and hydrolysis of Nd^{3+} from 30 to 290°C at saturated vapor pressure with in-situ pH_m measurement. In *Water-rock interactions, ore deposits and environmental geochemistry: A tribute to David A. Crerar*, (ed. R. Hellmann and S. A. Wood), Vol. 7, pp. 229–256. The Geochemical Society.

Wood S. A. and Ricketts A. (2000) Allanite-(Ce) from the Eocene Castro granite, Idaho: response to hydrothermal alteration. *Can. Mineral* **38,** 81–100.

Wood S. A. and Williams-Jones A. E. (1994) The aqueous geochemistry of the rare-earth elements and yttrium 4. Monazite solubility and REE mobility in exhalative massive sulfide-depositing environments. *Chem. Geol.* **115,** 47–60.

Young H. W (1985) Geochemistry and hydrology of thermal springs in the Idaho Batholith and adjacent areas, Central Idaho, pp. 44. USGS. Water Res. Inv. Rep.